Supplemental material

Carrasco-Rando et al., https://doi.org/10.1083/jcb.201810171

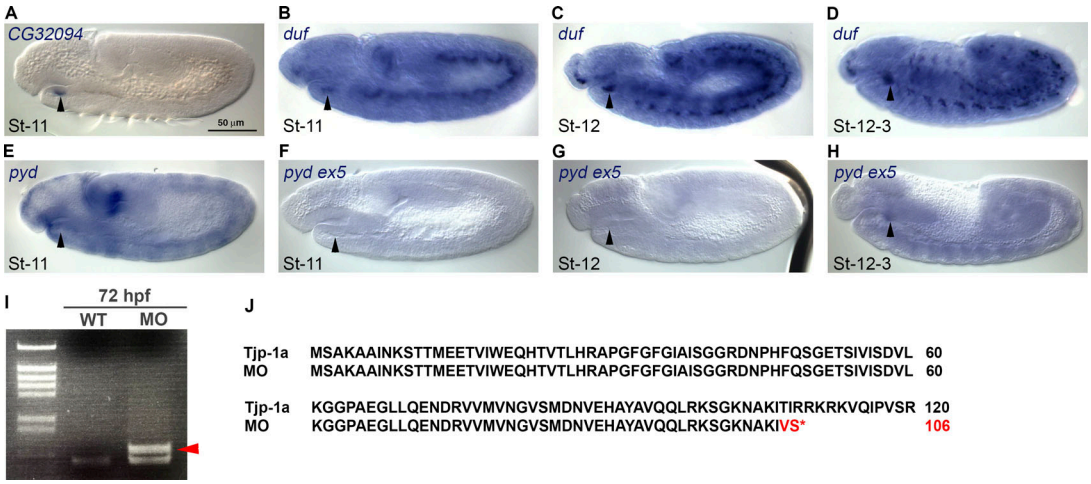

Figure S1. ***duf*is expressed earlier than *pyd* in nephrocytes. (A, B, E, and F)** The onset of *duf* expression in nephrocytes at stage 11, detected with a *duf* cDNA probe (B), coincides with that of *CG32094* (A; cDNA RH58005) and precedes *pyd* expression detected with a *pyd* cDNA probe (E) or a probe specific for *pyd*-exon 5 (F). **(C and G)** No expression of *pyd* is detected in nephrocytes at early stage 12, when *duf* is strongly expressed (C). **(D and H)** *pyd* expression in nephrocytes is delayed to stage 12-3. All panels show lateral views of embryos at the indicated developmental stages. In all cases, the arrowheads point to the position of the garland nephrocytes. **(I and J)** Morpholino MOex4 induces *tjp1a* missplicing visible as an increase in amplicon size (from 683 to 815 bp, red arrowhead in I) that leads to a truncation of the Tjp1a protein at amino acid 106 after misincorporation of two amino acids (J). Related to Figs. 1 and 3.

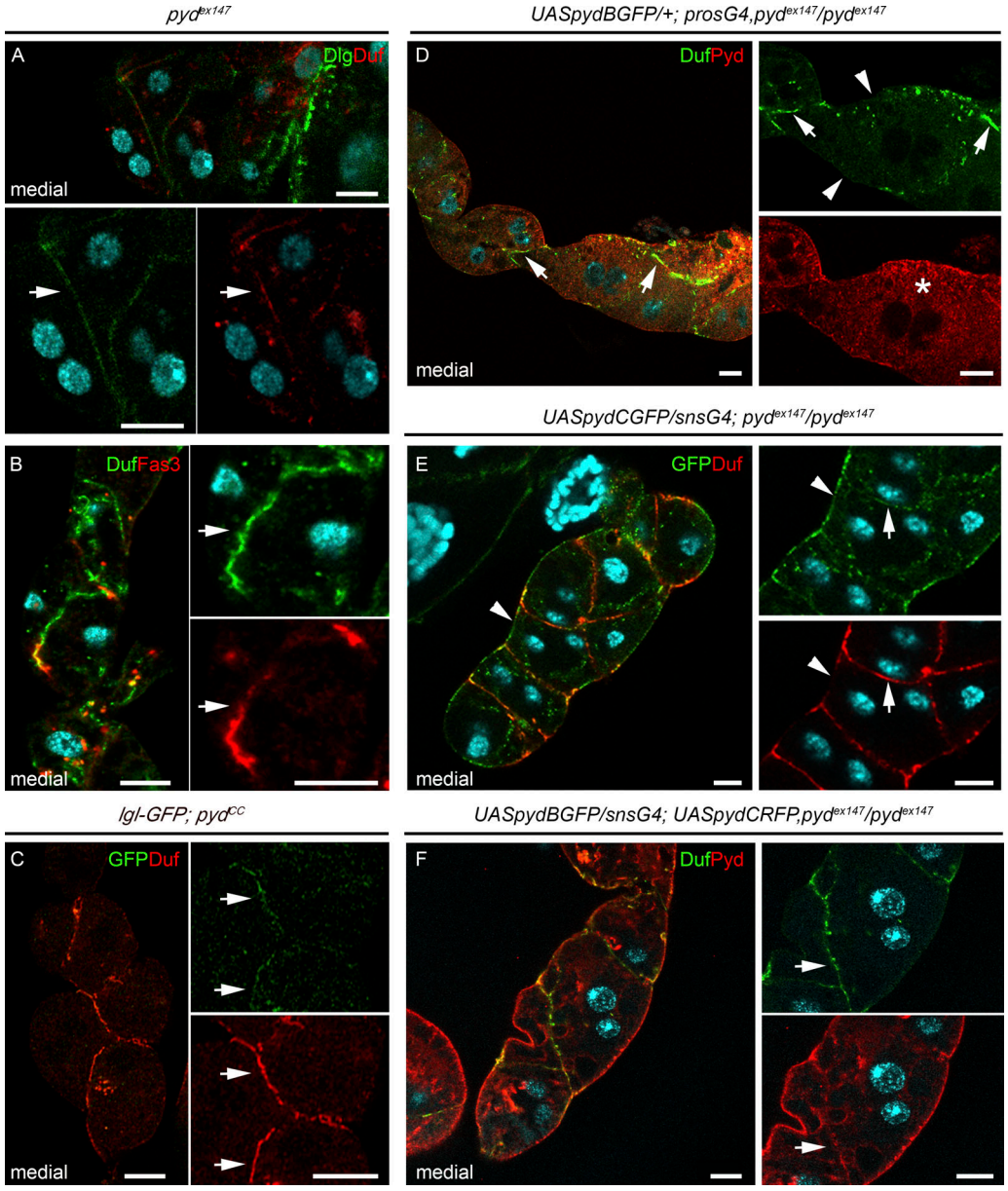

Figure S2. **Accumulation of junctional markers at cell contacts in *pyd* nephrocytes and failure to rescue *pyd* phenotypes with Pyd-B and Pyd-C isoforms. (A–C)** The septate junction markers Dlg, Fas3 and Lgl localize at ectopic junctional complexes in *pyd* nephrocytes. MT confocal sections of pyd^{ex147} nephrocytes (A and B) stained with Duf and Dlg or Fas3 antibodies and *lgl-GFP; pydCC6* nephrocytes stained with Duf and GFP antibodies (C), showing the presence of Dlg, Fas3, and Lgl at nephrocytes cell-cell contacts (arrows). **(D–F)** Pyd isoforms B and C fail to rescue *pyd* phenotype in nephrocytes. MT confocal sections of whole-mount pyd^{ex147} nephrocytes stained with Duf, and Pyd or GFP antibodies showing that neither the formation of SDs, nor the agglutination phenotype of pyd^{ex147} mutants is rescued by reintroduction of isoforms Pyd-B (D), Pyd-C (E), or both isoforms together (F) using two different drivers. Arrows point to accumulation of Duf (D–F) and Pyd-C (E and F) at junctions between agglutinated nephrocytes and arrowheads to absence of Duf at external membrane. Note that Pyd-C, but not Pyd-B, is present at the external membrane and that Pyd-B is homogeneously distributed throughout the cytoplasm (asterisks in D). Scale bars represent 10 µm. n = 19 nephrocytes in A, n = 24 in B, n = 33 in C, n > 104 in D, n > 334 in E, and n > 90 in F. Related to Figs. 1 and 5.

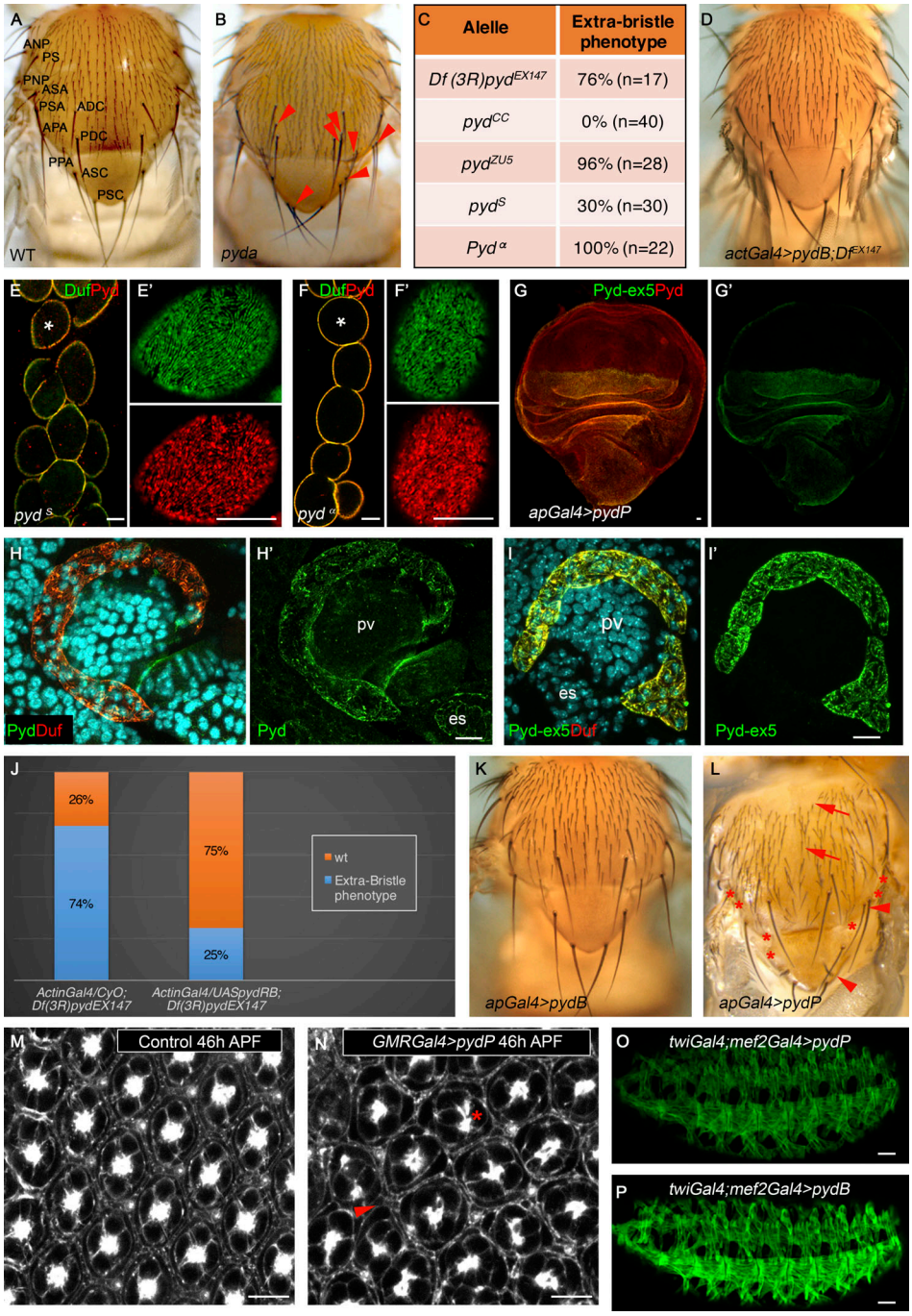

Figure S3. **Phenotypic characterization of novel *pyd* alleles. (A and B)** Dorsal views of WT and pyd^{α} nota showing the normal pattern of 11 macrochaetae per heminotum (A) and the extra-bristle phenotype in the mutant (arrowheads in B). **(C)** Quantification of extra-bristle phenotypes in *pyd* alleles indicated as a percentage of heminota presenting extra bristles. **(D and J)** Reintroduction of Pyd-B with *actin-Gal4* rescues the extra-bristle phenotype of pyd^{ex147} (n = 32 and 35 adults). **(E–F′)** Both pyd^{S} (E) and pyd^{α} (F) nephrocytes have WT densities of SDs (n = 35N/4S and 135N/12S, respectively). **(E and F)** MT confocal sections of representative strings of nephrocytes. **(E′ and F′)** External sections of the nephrocytes indicated with asterisks in E and F. **(G–I′)** Immunostaining of a larval wing disc overexpressing Pyd-P with *ap-GAL4* (G and G′) and stage-16 WT embryos (H–I′) to detect Pyd with an antibody that recognizes all isoforms (Pyd, G–H′) and with anti-Pyd-ex5, specific for Pyd-P (G, G′, I, and I′). Note that anti-Pyd-ex5 lightens the dorsal wing disc overexpressing Pyd-P (G and G′) and the garland nephocytes (H–I′) but does not react with other tissues such as the ventral compartment of the disc, the proventriculus (pv), or the esophagus (es). **(K and L)** Overexpression of Pyd-B (n = 21) with *ap-Gal4* has no phenotypic consequences on the bristle pattern (K), whereas that of Pyd-P (L, n = 13) induces lack of macrochaetae (asterisks), bristle duplications (arrowheads), and lower density of microchaetae, phenotypes similar to those derived from reduction of Delta activity (arrows, compare to A and de Celis et al., 1991). **(M and N)** Overexpression of Pyd-P in eye discs (*GMR-Gal4*) induces patterning defects, including an increase in the number of interommatidial and cone cells (arrowhead and asterisk in N; n = 6). **(O and P)** Pan-mesodermal overexpression of Pyd-P (O, n = 15) or Pyd-B (P, n = 13) does not affect muscle development. ANP, anterior notopleural; APA, anterior postalar; APF, after puparium formation; ASA, anterior supra-alar; ASC, anterior scutellar; PDC, posterior dorsocentral; PNP, posterior notopleural; PPA, posterior postalar; PSC, posterior scutellar. Scale bars represent 10 µm. Related to Figs. 5 and S2.

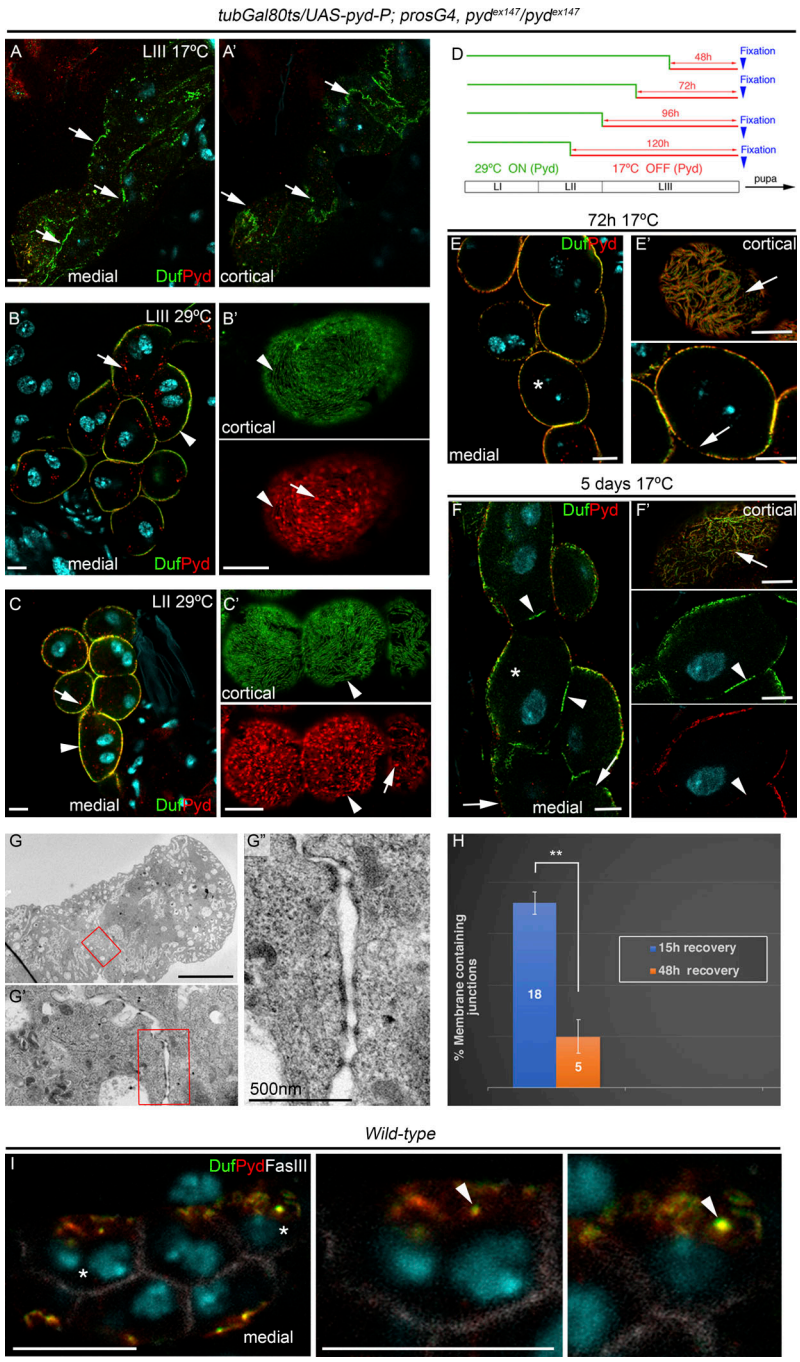

Figure S4. **Effects of the temporal manipulation of Pyd-P expression on the formation and stability of SDs. (A–C′)** Staining with Duf and Pyd antibodies of third- (A–B′) and second-instar (C and C′) larval nephrocytes of *w; tub-Gal80^{ts}/UAS-pyd-P; pros-Gal4, pyd^{ex147}/pyd^{ex147}* individuals grown at 17°C (A and A′) or 29°C (B–C′). **(A and A′)** In the absence of Pyd-P expression, no SDs are formed and Duf accumulates at cell junctions between agglutinated nephrocytes (arrows; *n* = 21N/2S). **(B and B′)** Experimental individuals cultured at 29°C until the third-instar larval stage present an almost complete rescue of SDs. Arrowheads point to accumulation of Duf and Pyd at the nephrocyte external membrane in a fingerprint-like pattern (*n* = 103N/10S). Excess of Pyd accumulates in internal and subcortical vesicles (arrows). **(C and C′)** At the second-instar larval stage, experimental individuals cultured at 29°C show an almost WT density of SDs (arrowheads) and excess of Pyd in vesicles (arrows; *n* = 81N/4S). These nephrocytes serve as control for the experiments shown in F. **(D)** Cartoon showing the experimental procedures used in E–G‴ to manipulate Pyd-P expression. **(E–F′)** Representative strings of nephrocytes (E and F) and details of the nephrocyte marked with the asterisk (E′ and F′) stained with Duf and Pyd antibodies. A mild (arrows in E′; *n* = 95N/10S) or strong (arrows in F and F′; *n* = 38N/4S) reduction in SD density can be observed after growing experimental individuals for 72 h (E and E′) or 120 h (F and F′) at 17°C in the absence of newly synthesized Pyd. Note the absence of extra Pyd in dots and the presence of only Duf at cell junctions between agglutinated nephrocytes (arrowheads in F and F′). **(G–G″)** TEM images of experimental larval nephrocytes after 120 h at 17°C. Note the presence of ectopic septate-like junctions between agglutinated nephrocytes (G′ and G″). **(H)** Quantification of the extent of membrane engaged in junctional complexes in experimental nephrocytes after 15 and 48 h of recovery at 29°C; *n* = 8 and 9 independent cell contacts, respectively. Error bars indicate SEM. **, P < 0.01 (two-tailed paired *t* test). **(I)** Stage 15 WT embryonic nephrocytes showing the presence of large vesicles containing Duf and Pyd (arrowheads). Asterisk indicates the cells shown at higher magnification. Unless indicated otherwise, scale bars represent 10 µm. Related to Fig. 6.

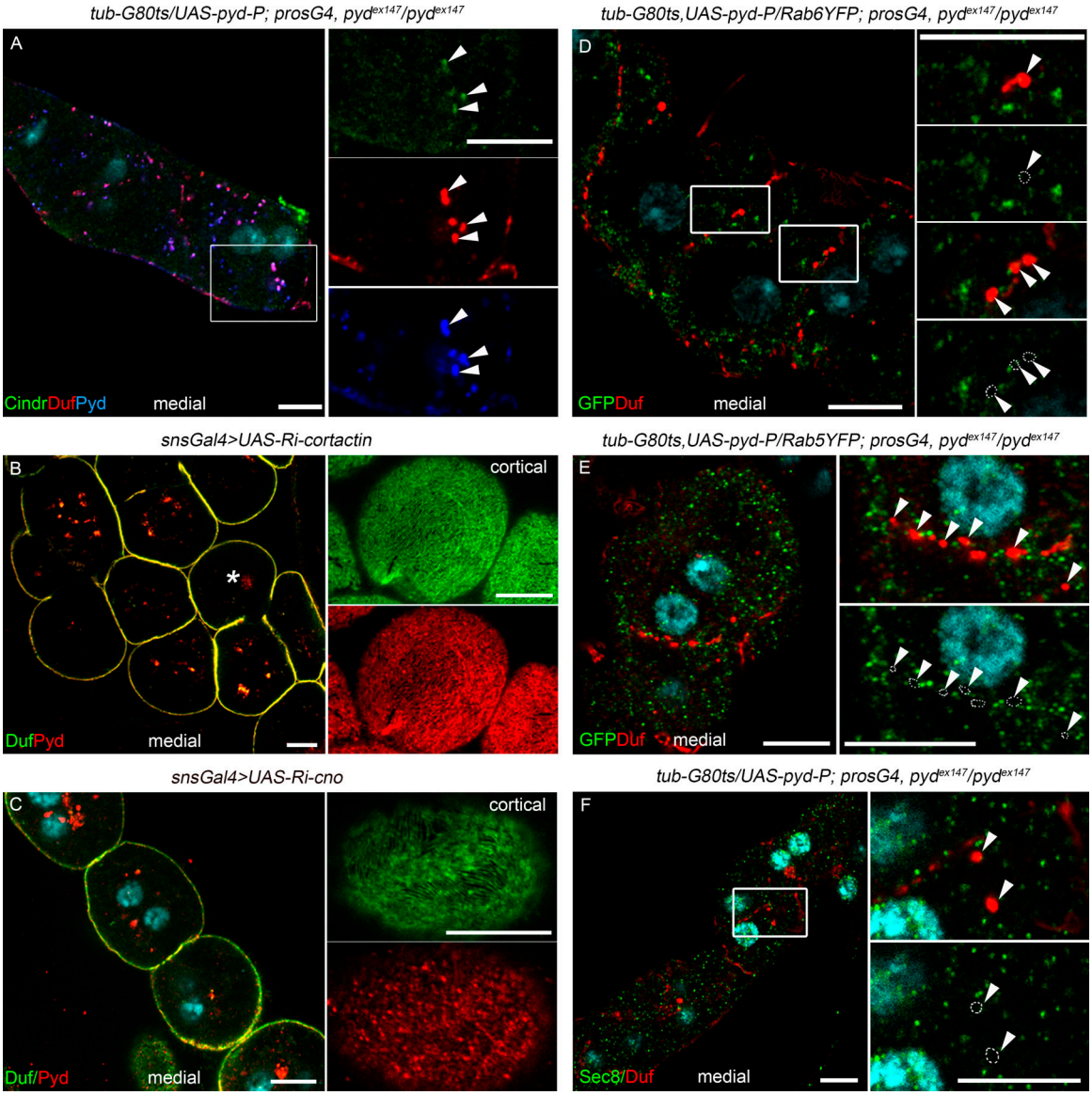

Figure S5. **Characterization of Duf vesicle content during SD recovery and dispensability of Cortactin and Cno for SD formation. (A)** Representative string of larval *tub-Gal80^{ts}/UAS-pyd-P; pros-Gal4, pyd^{ex147}/pyd^{ex147}*nephrocytes fixed after 24 h of recovery by expression of *UAS-Pyd-P* stained with Cindr, Duf, and Pyd antibodies. Note the colocalization of the three SD components in the vesicles (*n* = 24N/3S). **(B and C)** Larval nephrocytes stained with Duf and Pyd antibodies after attenuation of the cortical actin regulators Cortactin (B; *n* = 52N/4S) or Canoe (Cno; C, *n* = 30N/4S) showing normal density of SDs. **(D–F)** Larval *tub-Gal80^{ts}, UAS-pyd-P/Rab6YFP; pros-Gal4, pyd^{ex147}/pyd^{ex147}* (D; *n* = 27N/3S), *tub-Gal80^{ts}, UAS-pyd-P/Rab5YFP; pros-Gal4, pyd^{ex147}/pyd^{ex147}* (E, *n* = 28N/6S) or *tub-Gal80^{ts}/UAS-pyd-P; pros-Gal4, pyd^{ex147}/pyd^{ex147}* (F; *n* = 48N/6S) nephrocytes costained with Duf and GFP (D and E) or the exocytic marker Sec8 (F) antibodies showing exclusion of Rab6, Rab5, and Sec8 in the Duf-containing vesicles during recovery (arrowheads). Related to Fig. 7.

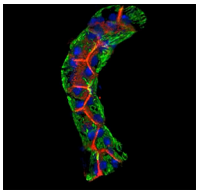

Video 1. **3D reconstruction of embryonic stage 16 WT nephrocytes.** Reconstruction using the 3DViewer plugin in Fiji of a representative string of nephrocytes stained for Duf (green), Fas3 (red), and DAPI (blue) in which part of the external surface has been deleted to gain access to internal structures. Frame rate: 6 frames per second. Related to Fig. 1.

Reference

de Celis, J.F., M. Marí-Beffa, and A. García-Bellido. 1991. Function of trans-acting genes of theachaete-scute complex in sensory organ patterning in the mesonotum of Drosophila. *Rouxs Arch. Dev. Biol.* 200:64–76. https://doi.org/10.1007/BF00637186